Theor Chim Acta (1989) 76: 7–31

Theoretica Chimica Acta

Molecular vibrations in a gradient extremal path

Norihiro Shida, Jan E. Almlöf, and Paul F. Barbara
Department of Chemistry, University of Minnesota, 207 Pleasant Street S.E., Minneapolis, MN 55455, USA

(Received October 26, 1988; revised and accepted January 26, 1989)

Summary. The calculation of vibrational states using a gradient extremal path is discussed. Gradient extremal paths are defined by local criteria, which lead to stable solutions. This has certain advantages in comparison with a steepest-descent path, which is often difficult to determine accurately. For cases where a reaction path formalism is applicable, a path based on the gradient extremal concept gives results in close agreement with those obtained using traditional steepest-descent methods. We present algorithms for carrying out such calculations and also give some numerical results.

Key words: Gradient extremal path — Molecular vibrations — Reaction path — Reaction coordinate

1. Introduction

The study of large amplitude molecular vibrations is important for understanding chemical reactions and rearrangement processes. For calculations of these vibrations, it is usually necessary to determine adiabatic potential surfaces in large regions of coordinate space, rather than force constants evaluated only at the equilibrium structures. A substantial calculational effort is required to attain sufficient accuracy for the electronic part of the potential. It is therefore desirable to reduce the number of points required to construct the potential surface without loss of the information necessary to describe the large amplitude vibration. This problem is usually solved by means of a reaction path approach, in which molecular vibrations are described in a narrow region along the path.

Calculations of chemical dynamics using a reaction path were first carried out in the 1960's. Pioneering work was done by Hofacker et al. [1] and by Marcus [2], who proposed a vibrationally adiabatic model using a natural collision coordinate. A more systematic method was established in the 1970's by Fukui [3], who used a steepest descent path in terms of a mass-weighted Cartesian coordinate system as a reaction coordinate; the "intrinsic reaction coordinate" (IRC). Their differential geometry techniques [4] increased the value of the method, and their group followed with some applied examples [5]. Truhlar and coworkers have also made extensive use of the IRC and have developed a variational transition state theory formalism for dynamics calculations based on the IRC [6]. From the early 1980's, Miller and coworkers have extended the work of Fukui, and proposed the reaction path Hamiltonian [7]. Hougen et al. [8] studied the couplings between rotations and vibrations, and derived the original rotational-bending (inversion) Hamiltonian using an internal coordinate as a reaction coordinate, and applied the method to some small molecules.

The original idea of a gradient extremal path (GEP) is due to Pancir [9], who proposed a path where the gradient vector is always an eigenvector of the Hessian matrix. Reaction paths based on that criterion were tested in simple model systems by Müller [10]. His conclusions were, however, rather pessimistic regarding the usefulness of the GEP concept. A rigid mathematical definition was given by Basilevsky et al. [11], who also proposed the physical interpretation of a GEP as a "a least ascent path". They concluded that the GEP and the IRC pass through the same points only where the norm of the gradient is zero (i.e. stationary points) or where the curvature of the IRC is zero. In other cases, the deviation between the GEP and the IRC is proportional to the curvature of the steepest descent path and to the square norm of the gradient. It is also inversely proportional to the square of the normal frequency for the corresponding bath mode, as will be discussed in the following section. In general, a reaction path approach gives a good description when the vibrational frequencies in the bath are high compared to that of the large amplitude vibration (this is a required condition for a *vibrational adiabatic model*). The couplings between the large amplitude and bath modes are expected to be small in this case and the vibrational amplitudes in the bath are also relatively small. When the above condition is satisfied, Basilevsky's analysis suggests that the GEP is close to the IRC.

In 1986, Hoffman et al. discussed the basic nature of GEPs [12] with emphasis on their usefulness for molecular dynamics. Their analysis shows that third-order derivatives play an important role for characterizing GEPs. Very recently, Jørgensen et al. [13] have developed efficient algorithms for finding transition states using the second order GEP, starting from an equilibrium geometry. To date this is the only application of GEPs to molecular structure.

One reason why the GEP concept requires attention is its interpretation as a least ascent path. It would thus seem to be more appropriate for describing the initial phase of chemical reactions than the IRC. An IRC is more naturally associated with the later state of a reaction (the requirement for microscopic reversibility will of course prevent the use of different paths for forward and

backward reactions). Another reason is the local criterion defining a GEP. Several schemes are in use for obtaining (approximate) IRCs in molecular systems. However, roundoff errors induced during numerical calculations tend to make an IRC unstable and inaccurately determined. There is no easy way to remove these roundoff errors, since no local criteria define an arbitrary point on an IRC.

In this work, we have used the GEP as a reaction path to describe large amplitude vibrations. In the following sections, we will discuss the methods and algorithms used, and present some numerical results for vibrational states of NH_3 and H_3O^+.

2. Gradient extremal path

The most rigid discussion of the GEP concept is due to Hoffman et al. [12] in 1986. Assuming an M-dimensional potential surface:

$$V = f(\boldsymbol{x}) = f(x_1, x_2, \ldots, x_M), \tag{2.1}$$

the term *contour subspace* is introduced to denote the $(M-1)$ dimensional subspace defined by the condition $f(\boldsymbol{x}) =$ constant. The GEP is defined as a path where the absolute value of the gradient is extremal on each contour subspace. Mathematically, it is defined as follows: The projection matrix ($\boldsymbol{P}^0$)

$$\boldsymbol{P}^0\boldsymbol{a} = \boldsymbol{a}\boldsymbol{P}^0 = \left\{\sum_j P^0_{ij} a_j\right\}, \tag{2.2}$$

projects an arbitrary vector $\boldsymbol{a}$ onto the direction which is parallel to the gradient. The explicit form of $\boldsymbol{P}^0$ is

$$\boldsymbol{P}^0 = \frac{|\nabla f\rangle\langle \nabla f|}{\langle \nabla f|\nabla f\rangle} \tag{2.3}$$

We will use the following notations for the gradient and the Hessian:

$$\boldsymbol{H}(\boldsymbol{x}) = (\nabla\nabla f(\boldsymbol{x})), \tag{2.4a}$$

$$\boldsymbol{g}(\boldsymbol{x}) = (\nabla f(\boldsymbol{x})). \tag{2.4b}$$

In this notation, $\boldsymbol{P}^0$ can be rewritten as

$$\boldsymbol{P}^0 = \frac{|\boldsymbol{g}\rangle\langle \boldsymbol{g}|}{g^2} \tag{2.3'}$$

The projection matrix, $\boldsymbol{P} = \boldsymbol{1} - \boldsymbol{P}^0$ projects an arbitrary vector onto the direction which is perpendicular to the gradient. In order to find the extremal condition of $|\boldsymbol{g}|$, one can now consider the variation of the square norm of $\boldsymbol{g}$, i.e.

$$\frac{\nabla(g^2)}{2} = \boldsymbol{H}\boldsymbol{g}. \tag{2.5}$$

This expression can be decomposed into directions which are parallel and perpendicular to the gradient. The parallel component is

$$\frac{\boldsymbol{P}^0\nabla(g^2)}{2} = \boldsymbol{P}^0\boldsymbol{H}\boldsymbol{g} = \lambda\boldsymbol{g}, \tag{2.6}$$

where λ has been defined as

$$\lambda = \frac{\boldsymbol{g}^T\boldsymbol{H}\boldsymbol{g}}{g^2}. \tag{2.6a}$$

Consequently,

$$\frac{\boldsymbol{P}\nabla(g^2)}{2} = \boldsymbol{H}\boldsymbol{g} - \lambda\boldsymbol{g}. \tag{2.7}$$

The gradient extremal is defined by the condition that (2.7) vanishes:

$$\boldsymbol{H}(\boldsymbol{x})\boldsymbol{g}(\boldsymbol{x}) = \lambda(\boldsymbol{x})\boldsymbol{g}(\boldsymbol{x}). \tag{2.8}$$

2.1. Second order GEP

Jørgensen et al. [13] have proposed a practical algorithm for obtaining the GEPs on multi-dimensional potential hypersurfaces in polyatomic molecules. The key point of their procedure is based on the method of trust region within which a potential surface is well described by a second order Taylor expansion. The advantage of their method is that the entire procedure is resolved into simple constrained optimizations using the molecular gradient and the Hessian matrix.

Their walking algorithm can be summarized as follows: Let $\boldsymbol{x}_k$ be a point on the GEP reached in the kth step of the walk. Our aim is to find the next point $(\boldsymbol{x}_{k+1})$, i.e. to determine the displacement vector, $\Delta\boldsymbol{x}_k$

$$\Delta\boldsymbol{x}_k = \boldsymbol{x}_{k+1} - \boldsymbol{x}_k. \tag{2.9}$$

In a sufficiently small region around $\boldsymbol{x}_k$, a second order Taylor expansion of the potential surface can be performed:

$$V^{(2)}(\boldsymbol{x}_k + \Delta\boldsymbol{x}_k) = V(\boldsymbol{x}_k) + \boldsymbol{g}^T(\boldsymbol{x}_k)\,\Delta\boldsymbol{x}_k + \tfrac{1}{2}\Delta\boldsymbol{x}_k^T\boldsymbol{H}(\boldsymbol{x}_k)\,\Delta\boldsymbol{x}_k. \tag{2.10}$$

In this region, the following simplifications apply for $\boldsymbol{H}$, $\boldsymbol{g}$ and λ (see (2.6a)):

$$\boldsymbol{H}(\boldsymbol{x}_k) = \boldsymbol{H}\,(\text{const}). \tag{2.11a}$$

$$\lambda(\boldsymbol{x}_k) = \lambda\,(\text{const}). \tag{2.11b}$$

$$\boldsymbol{g}(\boldsymbol{x}_k + \Delta\boldsymbol{x}_k) = \boldsymbol{g}(\boldsymbol{x}_k) + \boldsymbol{H}\,\Delta\boldsymbol{x}_k. \tag{2.11c}$$

At the point $\boldsymbol{x}_k + \Delta\boldsymbol{x}_k$, the following relation should be satisfied for the gradient extremal condition (see (2.8)):

$$(\boldsymbol{H} - \lambda\boldsymbol{1})\boldsymbol{H}\,\Delta\boldsymbol{x}_k = -(\boldsymbol{H} - \lambda\boldsymbol{1})\boldsymbol{g}. \tag{2.12}$$

Let $\boldsymbol{v}$ be the eigenvector of $\boldsymbol{H}$ belonging to λ:

$$(\boldsymbol{H} - \lambda \mathbf{1})\boldsymbol{v} = 0. \tag{2.13}$$

If λ is non-degenerate, a projection operator perpendicular to the gradient can be defined:

$$\boldsymbol{P} = \mathbf{1} - \boldsymbol{v}\boldsymbol{v}^T. \tag{2.14}$$

If $\boldsymbol{P}$ is applied to (2.12) from the left, one obtains

$$\boldsymbol{P}\boldsymbol{H}\,\Delta\boldsymbol{x}_k = -\boldsymbol{P}\boldsymbol{g}. \tag{2.15}$$

Since $[\boldsymbol{P}, \boldsymbol{H}] = 0$, we finally arrive at the following equation:

$$\Delta\boldsymbol{x}_k = -\boldsymbol{P}\boldsymbol{H}^{-1}\boldsymbol{g} + \boldsymbol{v}\boldsymbol{v}^T\,\Delta\boldsymbol{x}_k. \tag{2.16}$$

Introducing $\alpha = \boldsymbol{v}^T\,\Delta\boldsymbol{x}_k$, we can write (2.16) as

$$\Delta\boldsymbol{x}_k = -\boldsymbol{P}\boldsymbol{H}^{-1}\boldsymbol{g} + \alpha\boldsymbol{v}. \tag{2.17}$$

Jørgensen et al. used (2.17) for their potential surface walking algorithm. α is determined by their step size control algorithm [14], such that the new $\boldsymbol{x}_{k+1}$ point is still in the local region where a second order Taylor expansion is justified. The sign of α specifies the direction of the walk. If the sign is positive, the walk leads to a (local) energy minimum point. If α is negative, one will reach a saddle point.

2.2. GEP as a reaction coordinate

The GEP has the property that it always passes through the points where the absolute value of the gradient is extremal. In particular, all local energy minima and saddle points can be found by following (all) the GEPs on a surface. The GEP starting at a minimum energy point and following the direction of minimum gradient (one of the extremal conditions) in each contour subspace is a least ascent path from the minimum energy point.

It would seem natural that the GEP starting at the energy minimum point (reactant) continues to the saddle point (transition state). In fact, Jørgensen et al. carried out some numerical calculations for small molecules and demonstrated that the GEPs starting at the equilibrium geometries did indeed reach the transition states [13]. However, there are a number of different GEPs on a potential hypersurface (see [12]). Generally, it is not always true that the same GEP passes through the reactant, the transition state and the product of interest. This is not only a problem for GEP, but applies also to IRC paths. Nevertheless, the fact that the IRC approach has been successfully used in a large number of quantum [15] and semi-classical [16] applications encourages us to investigate also the GEP as a reaction path.

As the GEP is defined by local criteria, it can be calculated starting from any stationary point. The procedures of going up- and downhill can both be used and give identical results. This is a great advantage compared with the IRC, which is always defined starting from a saddle point, descending to a (possibly local) minimum point.

Equation (2.17) may be accurate enough for finding transition states. However, for a vibrational calculation, the path itself is important. In a true GEP, $\boldsymbol{PH}^{-1}\boldsymbol{g}$ is always zero. In (2.17), the old $\boldsymbol{PH}^{-1}\boldsymbol{g}$ in the kth iteration is used for the $(k+1)$th iteration. Generally, the approximate GEP calculated in actual applications using (2.17) tends to take a zigzag course about the true GEP. This problem can be remedied by using

$$\boldsymbol{x}'_k = \boldsymbol{x}_k - \boldsymbol{PH}_k^{-1}\boldsymbol{g}_k \tag{2.18}$$

instead of $\boldsymbol{x}_k$ for the reaction path.

3. The reaction path Hamiltonian

In a vibrational calculation using a reaction path, it is assumed that the large-amplitude vibrational mode is well described by a one-dimensional curvilinear coordinate. By this assumption, the higher order terms arising from other degrees of freedoms are neglected, and the classical total vibrational Hamiltonian can be approximated as

$$\mathscr{H}(r, p_r, \boldsymbol{q}, \boldsymbol{p}_q) = \tfrac{1}{2}(p_r \boldsymbol{p}_q^T)\begin{pmatrix} G_{rr} & \boldsymbol{G}_{rq} \\ \boldsymbol{G}_{qr} & \boldsymbol{G}_{qq} \end{pmatrix}\begin{pmatrix} p_r \\ \boldsymbol{p}_q \end{pmatrix} + V_0(r) + \boldsymbol{g}(r)^T(\boldsymbol{q} - \boldsymbol{q}_0) + \tfrac{1}{2}(\boldsymbol{q} - \boldsymbol{q}_0)^T\boldsymbol{H}(r)[\boldsymbol{q} - \boldsymbol{q}_0). \tag{3.1}$$

For the remaining degrees of freedoms ($\boldsymbol{q}$) (which we refer to as the *bath*), the potential energy contributions are approximated to second order terms along the reaction coordinate. The remaining problem is to determine the kinetic energy expression, i.e. the $\boldsymbol{G}$ matrix.

3.1. The steepest descent path

Before discussing the reaction path Hamiltonian of the GEP, let us consider that of the IRC [7], which is simpler. We first assume that the steepest descent reaction path ($\boldsymbol{S}(r)$) is already obtained in a mass weighted Cartesian coordinate system and that a normal vibrational analysis is also carried out along the reaction path in the $(3N-7)$ dimensional space. (The components parallel to the reaction path and the components corresponding to the translations and rotations are projected out. The Eckart condition [17] is the best criterion for the latter purpose, even though a complete removal of rotational components is not possible.) Since the tangent direction of the steepest descent path is always parallel to the gradient, no component of the gradient remains in the projected subspace. Therefore, if we introduce the normal coordinates ($\boldsymbol{Q}$) in the projected subspace, (3.1) can be written as

$$\mathscr{H}(r, p_r, \boldsymbol{Q}, \boldsymbol{p}_Q) = \tfrac{1}{2}(p_r \boldsymbol{p}_Q^T)\begin{pmatrix} G_{rr} & \boldsymbol{G}_{rQ} \\ \boldsymbol{G}_{Qr} & \boldsymbol{G}_{QQ} \end{pmatrix}\begin{pmatrix} p_r \\ \boldsymbol{p}_Q \end{pmatrix} + V_0(r) + \sum_{k=1}^{3N-7} \tfrac{1}{2}\omega_k^2(r)Q_k^2. \tag{3.2}$$

Consider the kinetic energy part of (3.2). An arbitrary point in a mass weighted Cartesian coordinate system ($\boldsymbol{X}$) can be expressed in terms of r and $\boldsymbol{Q}$:

$$\boldsymbol{X}_i = \boldsymbol{S}_i(r) + \xi_i = \boldsymbol{S}_i(r) + \sum_{k=1}^{3N-7} \boldsymbol{L}_{ik}(r)Q_k, \tag{3.3}$$

$$\boldsymbol{X}_i = \{\sqrt{m_i}x_i, \sqrt{m_i}y_i, \sqrt{m_i}z_i\}, \tag{3.4}$$

where $\boldsymbol{S}$ is the reaction path, ξ is the small displacement from the reaction path and $\boldsymbol{L}$ is the transformation matrix from normal coordinates $\boldsymbol{Q}$ to mass weighted Cartesian coordinates $\boldsymbol{X}$. The classical kinetic energy in terms of momenta in the mass-weighted Cartesian coordinate system can be written as

$$T = \sum_{i=1}^{N} \tfrac{1}{2}\boldsymbol{p}_{\dot{x}_i}^2. \tag{3.5}$$

T can be expressed in terms of (P_r, $\boldsymbol{P}_Q$) by canonical transformations [18] using the relations in (3.3). The final results is as

$$T = \sum_{k=1}^{3N-7} \tfrac{1}{2}p_k^2 + \left[\frac{\left[p_r - \sum_{k,1=1}^{3N-7} Q_k p_1 B_{k1}(r)\right]^2}{\left[1 + \sum_{k=1}^{3N-7} Q_k B_{k\,3N-6}(r)\right]^2}\right], \tag{3.6}$$

where B_{ij} is defined as follows.

$$B_{ij} = \sum_{m=1}^{N} \boldsymbol{L}'_{mi}(r)\boldsymbol{L}_{mj}(r) \qquad (j = 1, 3N-7), \tag{3.7a}$$

$$B_{i\,3N-6} = \sum_{m=1}^{N} \boldsymbol{L}'_{mi}(r)\boldsymbol{S}'_m(r). \tag{3.7b}$$

One advantage of the steepest descent reaction path is obvious here. The IRC always follows the direction of the gradient, which leads to two important simplifications:

1. The bath is always orthogonal to the reaction path.
2. There are no rotational or translational components induced.

3.2. The gradient extremal path

Based on the definition (2.8), one may be led to assume that the GEP also follows the direction of the gradient. However, this is not the case. The tangent of a GEP always makes a finite angle to the gradient [11, 12]. In evaluating the expression for the Hamiltonian, one must therefore consider the remaining gradient component in the bath and the induced rotational and translational components of the reaction path.

In the second order GEP, the step vector $\Delta \boldsymbol{x}_k$ is expressed as a linear combination of the Hessian eigenvectors. To remove the rotational and translational

components, it is sufficient to remove these components from the Hessian matrix (see Appendix 1). Therefore, we define the projection operator, $\boldsymbol{P}_{rt}$ which projects an arbitrary vector onto the translational and rotational component space. To first order, the projected Hessian,

$$\boldsymbol{H}' = (\mathbf{1} - \boldsymbol{P}_{rt})\boldsymbol{H}(\mathbf{1} - \boldsymbol{P}_{rt}), \tag{3.8}$$

has no component in the space of rotations and translations.

The next problem is the remaining gradient components in the bath. There are several ways to address that problem:

The easiest way is to treat the gradient the same way as in the case of the IRC. In this case, the gradient vector still has a component in the bath. The reaction path Hamiltonian is changed to

$$\mathscr{H}(r, p_r, \boldsymbol{Q}, \boldsymbol{P}_Q) = \tfrac{1}{2}(p_r \boldsymbol{p}_Q^T) \begin{pmatrix} G_{rr} & \boldsymbol{G}_{rQ} \\ \boldsymbol{G}_{Qr} & \boldsymbol{G}_{QQ} \end{pmatrix} \begin{pmatrix} p_r \\ \boldsymbol{p}_Q \end{pmatrix} + V_0(r) + \sum_{k=1}^{3N-7} f_k(r) Q_k + \sum_{k=1}^{3N-7} \tfrac{1}{2}\omega_k^2(r) Q_k^2. \tag{3.9}$$

This straightforward extension is practical and simple when the linear term, $\boldsymbol{f}$ is small. The fatal weakness of this approach is that some of the ω may become imaginary near the saddle point when $\boldsymbol{f}$ is not small. The Hessian matrix has one negative eigenvalue λ_{neg} in the region of the saddle point. The route to a nearby (possibly local) minimum is approximately parallel to the corresponding eigenvector $\boldsymbol{v}_{\text{neg}}$. In the IRC approach, $\boldsymbol{v}_{\text{neg}}$ is also a tangent of the reaction path. Therefore, no negative eigenvalues remain after the reaction path components have been projected out. If $\boldsymbol{f}$ is small, the same situation can be expected with the GEP since it also follows the direction of the gradient and has a trajectory similar to that of the IRC (the difference between GEP and IRC is discussed in Sect. 4). However, when $\boldsymbol{f}$ is not small, the tangent of the GEP can be rather different from the direction to the minimum. In this case, some components of $\boldsymbol{v}_{\text{neg}}$ do remain in the projected space and negative eigenvalues may arise in the bath. If this situation occurs, $\mathscr{H}$ in (3.9) is unbounded.

Even if there is some finite angle between the direction of the gradient vector and the tangent direction of the reaction path, the reaction path roughly follows the direction of the gradient, in order to reach the saddle point. Another approach is, therefore, to use the non-orthogonal bath where the gradient components, but not the reaction path components, are projected out. This procedure never encounters the difficulty described above. As the gradient vector is always an eigenvector of the Hessian, the new $\boldsymbol{Q}$ set in the bath can be obtained by just diagonalizing the Hessian matrix, $\boldsymbol{H}'$ in (3.8). In this model, the form of the reaction path Hamiltonian is the same as that of the steepest descent path in (3.2), but the ($\boldsymbol{G}$) matrix becomes more complicated.

Miller et al. derived the reaction path Hamiltonian for IRC [7a] using classical mechanics. An analogous expression can be derived quantum-mechanically as follows:

The kinetic energy operator in a mass-weighted Cartesian coordinate system

is expressed as

$$\mathscr{T} = -\sum_{\sigma}^{N} \frac{1}{2} \frac{\partial^2}{\partial \boldsymbol{X}_{\sigma}^2}. \tag{3.10}$$

The matrix element of $\mathscr{T}$ for an arbitrary *bra*, $\langle\varphi|$ and *key*, $|\chi\rangle$ can be written as follows in terms of general coordinates ($\boldsymbol{q}$) (see Appendix 2):

$$I = \langle\varphi|\mathscr{T}|\chi\rangle = \frac{1}{2}\int \sum_{j,k} a_{jk}^{-1} \frac{\partial\varphi^*}{\partial q_j} \frac{\partial\chi}{\partial q_k} J\left(\frac{\boldsymbol{X}}{\boldsymbol{q}}\right) d\boldsymbol{q}, \tag{3.11}$$

where the transformation $\boldsymbol{a}$ and the Jacobian, J are defined as

$$a_{jk} = \sum_{\sigma} \frac{\partial X_{\sigma}}{\partial q_j} \frac{\partial X_{\sigma}}{\partial q_k}, \tag{3.12a}$$

$$J\left(\frac{\boldsymbol{X}}{\boldsymbol{q}}\right) = \sqrt{|\boldsymbol{a}|}. \tag{3.12b}$$

The kinetic energy operator is then expressed as

$$\mathscr{T} = -\sum_{j,k} \frac{1}{2} \left(\frac{\partial}{\partial q_j}\right)^{\dagger} a_{jk}^{-1} \left(\frac{\partial}{\partial q_j}\right), \tag{3.13a}$$

$$\varphi^* \left(\frac{\partial}{\partial q_j}\right)^{\dagger} \equiv \frac{\partial\varphi^*}{\partial q_j}. \tag{3.13b}$$

It is easier to evaluate (3.13) in actual calculations than the more formal expressions [19], since no second derivatives of the wave function and no derivatives of $\boldsymbol{a}$ need to be evaluated.

It can easily be shown that the $\boldsymbol{a}^{-1}$ matrix in (3.13) corresponds exactly to the matrix $\boldsymbol{G}$ in (3.2). The explicit form of $\boldsymbol{a}$ can be determined directly from (3.3), (3.12a) (see Appendix 3).

The difference between Miller's reaction path Hamiltonian and ours is that (A3.7) is a more general expression for the $\boldsymbol{G}$ matrix used. If we apply the constraints (3.14), our formula agrees exactly with Miller's expression.

$$\sum_{\alpha} \frac{\partial \boldsymbol{S}_{\alpha}(r)}{\partial r} \boldsymbol{L}_{\alpha m}(r) = T_m(r) = 0, \tag{3.14a}$$

$$\sum_{m} \boldsymbol{L}_{\alpha m}(r)\boldsymbol{L}_{\beta m}(r) + \frac{\partial \boldsymbol{S}_{\alpha}(r)}{\partial r} \frac{\partial \boldsymbol{S}_{\beta}(r)}{\partial r} = \delta_{\alpha\beta}. \tag{3.14b}$$

(3.14a) enforces the orthogonality between the tangent direction of reaction path and the bath. (3.14b) represents the completeness of the orthonormalized $\{\boldsymbol{L}, \boldsymbol{S}'\}$ set.

$c(r)$, $\beta_m(r)$ and $R(r)$ are always unity in (A3.7). However, the evaluation of these expressions is still rather cumbersome. Therefore, one may instead use second-order Taylor expansions for (A3.7a)–(A3.7d). These results are shown in Appendix 4.

4. Deviations from the steepest descent path

Basilevsky et al. [11] discussed the deviation of the GEP from the corresponding steepest descent path for a two-dimensional system. Using the formulas in the previous section, we can estimate the deviation for a more general case.

The gradient extremal condition is defined by equating (2.7) to zero. It can be also written using the normal coordinates in (3.2) as

$$\frac{\partial(\boldsymbol{g}^2)}{\partial \boldsymbol{Q}_g} = 0, \tag{4.1}$$

where $\boldsymbol{Q}_g$ is a normal coordinate in the bath for the GEP reaction path. From the definition of a reaction path Hamiltonian in (3.2), $\boldsymbol{g}$ can be expressed in terms of r and $\boldsymbol{Q}_s$ for a steepest descent reaction path. Assuming that the direction of $\boldsymbol{Q}_g$ and $\boldsymbol{Q}_s$ are almost same, the approximate gradient extremal condition can be written as

$$\frac{\partial(\boldsymbol{g}^2)}{\partial \boldsymbol{Q}_s} \approx 0. \tag{4.2}$$

This condition can be evaluated as follows (see also Appendix 5):

$$\frac{\partial(\boldsymbol{g}^2)}{\partial \boldsymbol{Q}_i} = -2\left(\frac{\partial V_0(r)}{\partial r}\right)^2 u_i(r) + 2\frac{\partial V_0(r)}{\partial r}\omega_i(r)\frac{\partial \omega_i}{\partial r}Q_i + 2\omega_i^4(r)Q_i = 0. \tag{4.3}$$

The deviation of the GEP from the steepest descent path is estimated by the displacement of $\boldsymbol{Q}$ in (4.3):

$$Q_i = \frac{\left(\dfrac{\partial V_0(r)}{\partial r}\right)^2 u_i(r)}{\omega_i^4 + \dfrac{\partial V_0(r)}{\partial r}\omega_i(r)\dfrac{\partial \omega_i}{\partial r}}. \tag{4.4}$$

In (4.4), $(\partial V_0(r)/\partial r)^2$ represents the square norm of the gradient in the steepest descent path, $\boldsymbol{u}$ is the curvature partitioned among bath modes (see [7a], p. 103). $\boldsymbol{Q}$ becomes zero (i.e., the GEP and the steepest descent path pass through the same points) only when the gradient is zero or the steepest descent path is a straight line. In other cases, the difference is roughly inversely proportional to the fourth power of the bath frequencies. When a reaction path approach gives a good description and the vibrational adiabatic separation (which is discussed in the next section) is applicable, the bath frequencies are high, compared to that of the large-amplitude mode, and the GEP is therefore expected to be similar to the steepest descent path.

5. Adiabatic separations

Even though Eqs. (A4.1) become simpler than (A3.7), the Schrödinger equation is still difficult to solve due to its relatively high dimensionality. Marcus et al. proposed the vibrational adiabatic model [2], which is essentially analogous to a

zeroth Born–Oppenheimer separation between the reaction coordinate and the normal corrdinates in the bath. This approximation reduces the problem to a one-dimensional one. The contributions from the bath modes are included by adding their normal frequencies at each point to the one-dimensional potential energy along the reaction path. However, this procedure cannot be used exactly in the case of the GEP, since the path is not orthogonal to the bath, i.e. $\boldsymbol{T}(r)$ in (A3.6e) is not small with respect to some of the $\boldsymbol{Q}$ coordinates. In general, not all the normal coordinates have large $\boldsymbol{T}(r)$ values, but a few of them do. Therefore, we can divide the vibrational modes into three parts:

A. The large amplitude mode, which is described by the reaction coordinate;

B. Diabatic modes, those of the normal modes having large $\boldsymbol{T}(r)$ values;

C. Adiabatic modes, normal modes having small $\boldsymbol{T}(r)$ values.

Usually, the number of diabatic modes is small. A vibrational Schrödinger equation treating those modes and the reaction coordinate can be solved practically by methods such as the one described in the next section.

6. Basis set expansion

Several methods are available for solving the multi-dimensional Schrödinger equation for vibrational states. We have used the basis set expansion method, which is similar to the MCSCF method for electronic states.

For each degree of freedom ξ_j (ξ_j represents r and $\boldsymbol{Q}$ in this case) we introduce a set of Gaussian basis functions

$$\phi_{j,i}(\zeta_j) = (\zeta_j - \zeta_{j_0})^{n_{i,j}} \exp(-b_{i,j}(\zeta_j - \zeta_j^0)^2), \tag{6.1a}$$

where $b_{i,j}$ are harmonic exponents to be optimized and $n_{i,j}$ are non-negative integers chosen according to usual criteria. From these functions, we form many-dimensional product basis functions of the form

$$\psi_{\boldsymbol{i}}(\xi_1, \xi_2, \ldots, \xi_n) = \prod_j \phi_{j,i_j}(\xi_j), \tag{6.1b}$$

where $\boldsymbol{i} = (i_1, i_2, i_3, \ldots)$. The total vibrational wavefunction can now be expanded as

$$\Psi(\xi_1, \xi_2, \ldots, \xi_n) = \sum_{\boldsymbol{i}} C_{\boldsymbol{i}} \psi_{\boldsymbol{i}}(\xi_1, \xi_2, \ldots, \xi_n), \tag{6.2}$$

where $C_{\boldsymbol{i}}$ are expansion coefficients to be optimized together with the harmonic exponents, b_{ij}.

The next step is the orthonormalization of the product functions $\psi_{\boldsymbol{i}}$. For this purpose, it is sufficient to orthonormalize the one-dimensional functions $\{\phi\}$ for each individual j. Using the symmetric orthogonalization method [20], the

orthonormalized new sets, $\{\phi'\}$ and $\{\psi'\}$ are as follows:

$$\phi'_{j,i}(\xi_j) = \sum_k \phi_{j,k}(\xi_j) u^{(j)}_{k,i} \frac{1}{\sqrt{\varepsilon^{(j)}_i}}, \tag{6.3a}$$

$$\psi'_i(\xi_1, \xi_2, \ldots, \xi_n) = \prod_j \phi'_{j,i_j}(\xi_j), \tag{6.3b}$$

$$\Psi(\xi_1, \xi_2, \ldots, \xi_n) = \sum_j C'_i \psi'_i(\xi_1, \xi_2, \ldots, \xi_n), \tag{6.3c}$$

$$\boldsymbol{S}^{(j)} \boldsymbol{u}^{(j)} = \boldsymbol{u}^{(j)} \varepsilon^{(j)}, \tag{6.3d}$$

where $\boldsymbol{S}^{(j)}$ is the overlap matrix for the one-dimensional basis functions representing ξ_j.

For the optimization of the variational parameters, a two-step scheme is used, neglecting the couplings between $\boldsymbol{C}$ and $\boldsymbol{b}$, since the number of configurations becomes rather large. This procedure is almost the same as the MCSCF procedure for electronic states. The CI part is written as

$$\boldsymbol{HC} = \boldsymbol{EC}. \tag{6.4}$$

We can write the Hamiltonian symbolically as

$$\mathscr{H} = \mathscr{T} + \mathscr{V} = \sum_i \prod_j \mathscr{t}^{(j)}_i(\xi_j) + \sum_i \prod_j v^{(j)}_i(\xi_j) = \sum_i \prod_j \mathscr{h}^{(j)}_i(\xi_j). \tag{6.5}$$

The $\boldsymbol{H}$ matrix can be expressed as

$$H_{mn} = \langle \psi'_m | \mathscr{H} | \psi'_n \rangle = \sum_i \prod_j \langle \phi'_{j,m_j}(\xi_j) | \mathscr{h}^{(j)}_i(\xi_j) | \phi'_{j,n_j}(\xi_j) \rangle. \tag{6.6}$$

The gradient vector ($\boldsymbol{G}$) and the Hessian matrix ($\boldsymbol{H}$) in terms of the harmonic exponents are expressed as

$$(\boldsymbol{G})_i = \boldsymbol{C}^\dagger \frac{\partial \boldsymbol{H}}{\partial b_i} \boldsymbol{C} - \langle E \rangle \boldsymbol{C}^\dagger \frac{\partial \boldsymbol{S}}{\partial b_i} \boldsymbol{C}, \tag{6.7a}$$

$$(\boldsymbol{H})_{ij} = \boldsymbol{C}^\dagger \frac{\partial^2 \boldsymbol{H}}{\partial b_i \partial b_j} \boldsymbol{C} - \boldsymbol{C}^\dagger \frac{\partial \boldsymbol{H}}{\partial b_i} \frac{\partial \boldsymbol{S}}{\partial b_j} \boldsymbol{C} - \boldsymbol{C}^\dagger \frac{\partial \boldsymbol{H}}{\partial b_i} \frac{\partial \boldsymbol{S}}{\partial b_j} \boldsymbol{C}$$

$$+ 2\langle E \rangle \boldsymbol{C}^\dagger \frac{\partial \boldsymbol{S}}{\partial b_i} \frac{\partial \boldsymbol{S}}{\partial b_j} \boldsymbol{C} - \langle E \rangle \boldsymbol{C}^\dagger \frac{\partial^2 \boldsymbol{S}}{\partial b_i \partial b_j} \boldsymbol{C}, \tag{6.7b}$$

where $\langle E \rangle$ and $\boldsymbol{C}$ are eigenvalues and -vectors of the CI part. The explicit form of $\boldsymbol{G}$ and $\boldsymbol{H}$ can be easily obtained.

7. Numerical calculations

Numerical calculations were carried out for various vibrational states of H_3O^+ and NH_3 in order to check the accuracy of the method.

7.1. *Molecular vibrations in NH_3*

A number of theoretical and experimental studies on NH_3 have been reported, making this molecule a suitable example system. In this work, we used a simple SCF potential surface, since previous work [21] indicates that SCF calculations give quantitatively reasonable results. The basis set used was the MAXI-1 by Tatewaki [22], with two *d*-type polarization functions on N and a *p*-type polarization function on H added. Using this scheme, and analytical molecular gradients and Hessians, the GEP was calculated directly in a mass-weighted Cartesian coordinate system.

The calculated equilibrium geometry and some properties are given in Table 1, together with previous theoretical results [21] and experimental values [23]. The calculated properties are quite similar, indicating that our potential surface forms a realistic basis for the further treatment of vibrational structure.

Figure 1 shows the GEP in the subspace of A_1 symmetry, together with full potential surface in this space. The GEP is a smooth curve passing through the two equilibrium geometries and the saddle point. The curvature becomes larger as the angle increases. The steepest descent path and the GEP are indistinguishable on the scale of this figure. The angles between the tangent direction of the GEP and the direction of the gradient along the GEP are shown in Table 2. The angles are always very small (for the steepest descent path, the angles are zero by construction). The normal frequencies at the equilibrium geometry and at the saddle point are shown in Table 3. The following notation is used for the vibrational modes:

θ: A_1 bending mode;
ρ: A_1 stretching mode;
u: E asymmetric stretching mode;
w: E wagging mode.

Table 1. Computed properties for the NH_3 molecule in a.u.

	This work	Stevens [21]	Exp. [23]
Total energy	−56.197774	−56.22113	
Equilibrium geometry			
R(O—H)	1.894	1.892	1.912
Deviation from planarity	21.80°	22.57°	22.12°
Saddle point			
R(O—H)	1.865	1.861	
Deviation from planarity	0.00°	0.00°	
Inversion barrier (kcal/mol)	6.01	5.89	5.77

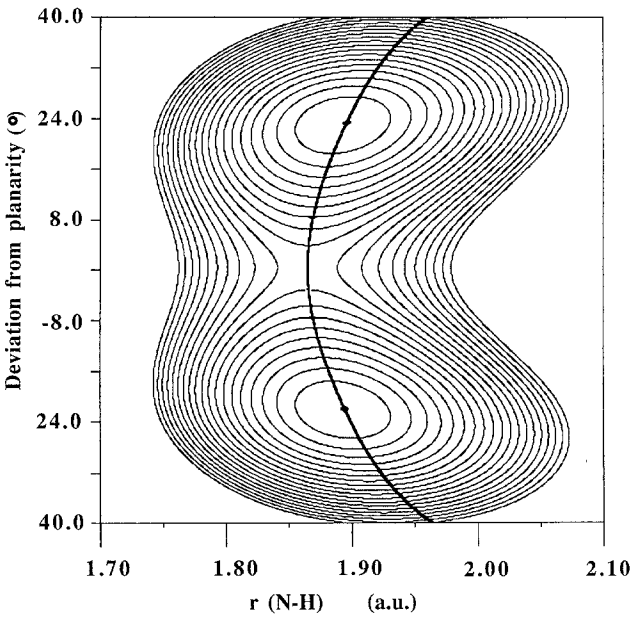

Fig. 1. The potential surface and the gradient extremal path in the (ρ, θ) space for NH_3. Each contour line: 0.001 (a.u.)

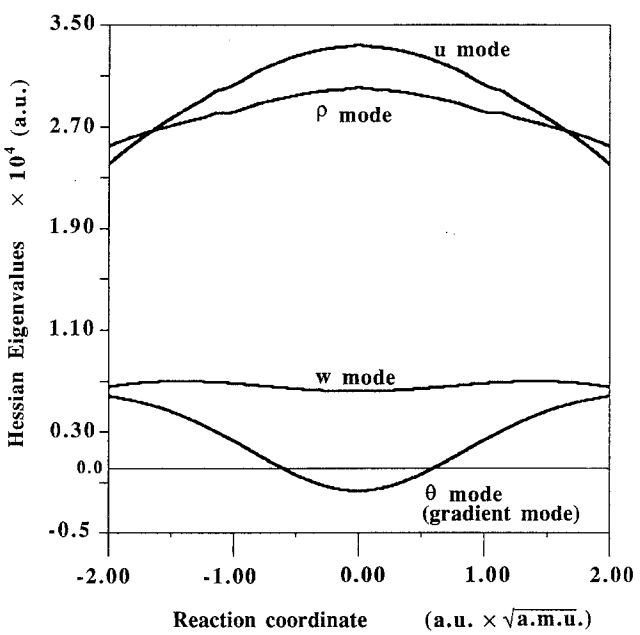

Fig. 2. The variation of Hessian eigenvalues along the reaction path in NH_3.

θ has an imaginary frequency at the saddle point. Frequencies corresponding to the bath are changing by 100–200 cm^{-1} between the equilibrium geometry and saddle point. In Fig. 2, the changes of the Hessian eigenvalues are plotted against the reaction coordinate of the GEP. The mode having a negative eigenvalue at the saddle point is the one parallel to the gradient. The next lowest eigenmodes

Table 2. Angle between the tangent of the GEP and the direction of the gradient in NH_3. $r = 1.123$ is the equilibrium geometry, $r = 0.0$ is the saddle point

Reaction coordinate (a.u. $\times \sqrt{\text{a.m.u.}}$)	Angle (°)
0.000	0.0
0.200	0.2
0.400	0.4
0.600	0.4
0.800	0.4
1.000	0.2
1.123	0.0
1.223	0.2
1.423	0.5
1.623	0.9
1.822	1.1
2.022	0.8

Table 3. Normal frequencies of NH_3 at the equilibrium geometry and the saddle point in cm^{-1}

	Equilibrium geometry	Saddle point
θ	1159	937(i)
ρ	3666	3793
u_1	3782	4002
u_2	3782	4002
w_1	1800	1703
w_2	1800	1703

Table 4. Vibrational frequencies for NH_3 in the two-dimensional system (θ, ρ) in cm^{-1}

n_ρ	n_θ	Exact Hamiltonian	GEP	IRC
0	0^+	0	0	0
0	0^-	0.9	1.0	1.0
0	1^+	1027	1012	1011
0	1^-	1069	1056	1056
0	2^+	1740	1730	1730
0	2^-	2069	2060	2059

Table 5. Diabatic effects on the vibrational frequencies from the ρ mode in NH_3 in cm^{-1}

n_ρ	n_θ	Diabatic	Adiabatic	None
0	0^+	0	0	0
0	0^-	1.0	1.0	1.2
0	1^+	1012	1012	996
0	1^-	1056	1056	1047
0	2^+	1730	1731	1703
0	2^-	2060	2060	2050

(which are twofold degenerate) correspond to the w modes. The highest two are the ρ and u modes. The variations of Hessian eigenvalues are largest in the u modes causing a crossing between the ρ mode and the u mode.

The calculated vibrational frequencies for the A_1 subsystem are summarized in Table 4 together with the frequencies using the two-dimensional exact Hamiltonian and the IRC. The agreement between the GEP and the exact Hamiltonian (EH) calculations is satisfactory. These results suggest that the GEP approach is appropriate for this system. Since the IRC and the GEP are very similar, the IRC is also appropriate, and gives almost the same frequencies as the GEPs.

In Table 5, the diabatic effects have been investigated. *Diabatic* is a two-dimensional calculation treating the reaction path Hamiltonian exactly, *adiabatic* is the one-dimensional calculation where the bath is treated adiabatically and in *none* the bath has been neglected completely. Obviously, the diabatic effects are

Table 6. Vibrational frequencies for NH_3 including the effects from all the bath modes in cm^{-1}

n_ρ n_θ	n_{u_1} n_{u_2}	n_{w_1} n_{w_2}	Adiabatic	Exp. [23]
0^+ 0	0 0	0 0	0	0.0
0^- 0	0 0	0 0	0.7	0.7934
1^+ 0	0 0	0 0	1034	932.44
1^- 0	0 0	0 0	1066	968.04

negligibly small, whereas it is important to include the effects from the bath adiabatically.

The vibrational frequencies including the effects from all the bath modes are summarized in Table 6. The inversion splitting agrees very well with the experimental value.

7.2. Molecular vibrations in H_3O^+

In the previous section, we analyzed various aspects of our method by treating the bending vibrational states of NH_3 molecule. The inversion splitting is, however, too small for a meaningful comparison. The H_3O^+ ion has almost the same structure as NH_3, but a much larger inversion splitting.

The potential surface was obtained using the SCF method. The basis set used in this calculations was the MIDI4 [24] by Tatewaki et al., with a *d* type polarization function and a *p* on hydrogen. Partly fortuitously, this calculation gives an inversion barrier of 2.06 kcal/mol, very close to the results of much more accurate studies [25].

Figure 3 shows the GEP and the potential surface in the A_1 subspace. The potential surface and the GEP are similar to those of NH_3 (see Fig. 1). However, the potential coupling becomes smaller and the GEP is almost a straight line in this case. Again, there is no visible difference between the GEP and the IRC.

The normal frequencies at the equilibrium geometry and at the saddle point are summarized in Table 7. These frequencies resemble those of NH_3 (see Table 3). However, the change of the bath frequencies between equilibrium and the saddle point is smaller than in NH_3, since the equilibrium structure is closer to the saddle point geometry. Still, the bath vibrations have a significant effect on the inversion splitting.

Table 8 summarizes the results obtained with the exact Hamiltonian, the GEP and the IRC in the A_1 subspace. The agreement between the exact calculations and the GEP is encouraging. (The frequency of the $(0, 1^+)$ state is already larger than the barrier height and there is no more doubling above this state.) The IRC and the GEP give almost the same frequencies, as was the case for NH_3.

The influence from the bath is summarized in Table 9a–c, where the effects from the ρ, u, and w modes are considered separately. In each table, the diabatic

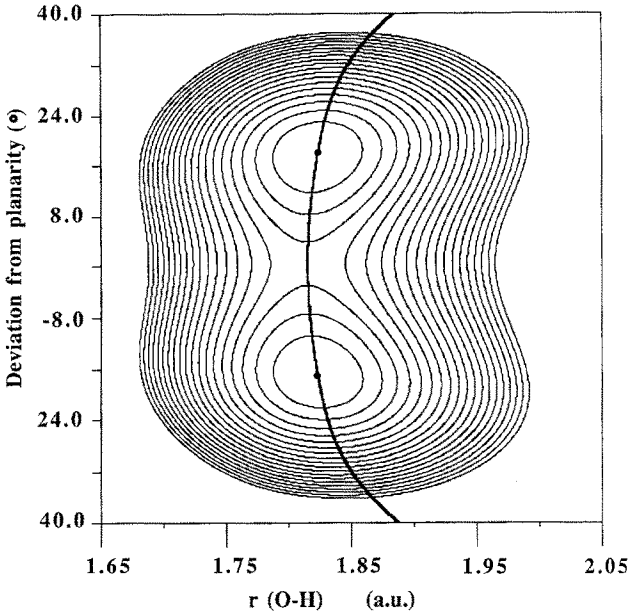

Fig. 3. The potential surface and the gradient extremal path in the (ρ, θ) space for H_3O^+. Each contour line: 0.001 (a.u.)

Table 7. Normal frequencies for H_3O^+ at the equilibrium geometry and the saddle point in cm^{-1}

	Equilibrium geometry	Saddle point
θ	934	704(i)
ρ	3835	3830
u_1	3946	4012
u_2	3946	4012
w_1	1785	1675
w_2	1785	1675

Table 8. Vibrational frequencies for H_3O^+ in the two dimensional system (θ, ρ) in cm^{-1}

n_ρ	n_θ	Exact Hamiltonian	GEP	IRC
0	0^+	0	0	0
0	0^-	60	64	64
0	1^+	606	608	608
0	1^-	1004	1016	1015
0	2^+	1555	1573	1573
0	2^-	2158	2187	2186

and the adiabatic calculation give almost the same energies. The diabatic effects are always negligibly small, as in the case of NH_3. One interesting result is the remarkable differences of the inversion doublings. Evidently, the effects from the bath are important for the inversion splitting in H_3O^+.

8. Summary and conclusions

We have reported calculations of vibrational states using a gradient extremal reaction path (GEP).

By virtue of the local criteria for such a path, its evaluation is more stable

Table 9a–c. Diabatic effects from the $r(a)$, $u(b)$ and $w(c)$ modes on the vibrational frequencies in H_3O^+ in cm^{-1}

a) n_ρ	n_θ	Diabatic	Adiabatic
0	0^+	0	0
0	0^-	64	64
0	1^+	608	608
0	1^-	1016	1015
b) n_{u_1}	n_{u_2} n_θ		
0 0	0^+	0	0
0 0	0^-	52	52
0 0	1^+	614	614
0 0	1^-	996	997
c) n_{w_1}	n_{w_2} n_θ		
0 0	0^+	0	0
0 0	0^-	82	83
0 0	1^+	597	598
0 0	1^-	1030	1032

and easier than the IRC. It may also be computationally less expensive, if computer codes are available for the efficient analytic evaluation of molecular Hessians. While the IRC can be also determined more efficiently when the Hessian is available, there is no local criterion and therefore no way to correct for successive buildup of inaccuracy in an IRC trajectory. In contrast, from a point approximately on the GEP one can always easily step back to the true GEP (even if the second order algorithm is not enough, the constrained optimization procedure in (2.18) can be repeated until the true GEP criteria are fulfilled). This permits a larger step length and a more reliable path calculation than for the IRC.

Furthermore, for a vibrational calculation it is necessary to know the path also in the repulsive walls (outside the minimum points). The IRC path essentially cannot meet that requirement; in contrast, there is no problem to obtain the GEP for the repulsive walls.

The reaction path Hamiltonian of the GEP becomes slightly more complicated than that of the IRC because of the non-orthogonality between the reaction path and the bath. However, the additional terms in the Hamiltonian can easily be evaluated and are expected to be small in cases when the reaction path model is valid.

The numerical applications to the inversion vibrational states of NH_3 and H_3O^+ indicate that:

1. The GEPs were virtually indistinguishable from the IRC. The formal estimate of the deviation between a IRC and a GEP suggest that they ought to be very similar whenever a one-dimensional treatment of the reaction is appropriate.

2. A one-dimensional GEP treatment gives vibrational frequencies very close to those obtained with the exact Hamiltonian.

3. The effects from the bath, which are important for the inversion splitting of H_3O^+, are well described by an adiabatic treatment.

Based on these experiences, it is reasonable to assume that a GEP would often be an attractive alternative to the traditional steepest descent path (IRC) for a one-dimensional treatment of a reaction process. Applications to systems such as $Cl + H—Cl \rightarrow Cl—H + Cl$ where the reaction path is strongly curvilinear are planned to test these assumptions.

Acknowledgements. The authors are grateful to Dr. T. Helgaker for his help with the modification of the SIRIUS–ABACUS program system [26, 27] and the discussions about this method, and to Mr. M. Feyereisen for assistance with the drawing programs. The authors also acknowledge valuable discussions with Profs. D. Truhlar and P. Jørgensen. This work was supported by the National Science Foundation, the Petroleum Research Fund, the Minnesota Supercomputer Institute and the UNISYS corporation. All the calculations were carried out on a Cray-2 computer at the Minnesota Supercomputer Center.

Appendix 1

Equation (3.3) applies to a molecule-fixed coordinate system. The relationship between a molecule- and a space-fixed coordinate system is

$$\boldsymbol{X}_{s,i} = \boldsymbol{X}_{G,i} + \Theta(\chi, \theta, \phi)^{-1}\boldsymbol{X}_i = \boldsymbol{X}_{G,i} + \Theta(\chi, \theta, \phi)^{-1} \times \left(\boldsymbol{S}_i(r) + \sum_{k=1}^{3N-7} \boldsymbol{L}_{ik}(r)Q_k\right) \qquad (i = 1, N), \tag{A1.1}$$

where $\boldsymbol{X}_s$, is an arbitrary point in a spaced fixed mass weighted Cartesian coordinate system, $\boldsymbol{X}_G$ is the center of mass in this coordinate system, Θ is the transformation matrix between the two coordinate system and (χ, θ, ϕ) are the Euler angles. To satisfy the condition that $\boldsymbol{X}_G$, Θ and $\boldsymbol{X}$ represent pure translations, rotations and vibrations, respectively, the following relations must be fulfilled:

$$\sum_{i=1}^{N} \sqrt{m_i}\boldsymbol{X}_i = 0, \tag{A1.2a}$$

$$\sum_{i=1}^{N} \boldsymbol{X}_i \times \dot{\boldsymbol{X}}_i = 0. \tag{A1.2b}$$

Sufficient conditions for (A1.2a) to be satisfied are

$$\sum_{i=1}^{N} \sqrt{m_i}\boldsymbol{S}_i(r) = 0, \tag{A1.3a}$$

$$\sum_{i=1}^{N} \sqrt{m_i}\boldsymbol{L}_{ik}(r) = 0. \tag{A1.3b}$$

Equation (A1.3b) is automatically satisfied in our procedures since we use the projected Hessian matrix, $\boldsymbol{H}'$ in (3.8). The reaction path $\boldsymbol{S}$ is determined from (2.9), (2.17), (2,18). In each step, the step vector is a linear combination of eigenvectors of the projected Hessian matrix. Therefore, there is no degree of freedom with respect to rotational and translational components in the step vector. For this reason, (A1.3a) is automatically satisfied. It is usually impractical to satisfy (A1.2b) exactly. As $\boldsymbol{LQ}$ is assumed to be a small displacement from the reaction path, we adopt the Eckart condition instead of (A1.2b). Sufficient conditions are

$$\sum_{i=1}^{N} \boldsymbol{S}_i(r) \times \boldsymbol{S}'_i(r) = 0, \tag{A1.4a}$$

$$\sum_{i=1}^{N} \boldsymbol{S}_i(r) \times \boldsymbol{L}'_{ik}(r) = 0. \tag{A1.4b}$$

These two equations are automatically satisfied for reasons described above.

Appendix 2

The matrix element of the kinetic energy integral for an arbitrary *bra*, $\langle\varphi|$ and *ket*, $|\chi\rangle$ is

$$I = \langle\varphi|\mathscr{T}|\chi\rangle = \langle\varphi| - \sum_{\sigma}^{N} \frac{1}{2}\frac{\partial^2}{\partial \boldsymbol{X}_\sigma^2}|\chi\rangle = -\frac{1}{2}\int \sum_{\sigma} \varphi^* \frac{\partial^2 \chi}{\partial^2 X_\sigma}\, d\boldsymbol{u}$$

$$= \left[-\frac{1}{2}\sum_{\sigma} \varphi^* \frac{\partial \chi}{\partial X_\sigma} \right]_{-\infty}^{+\infty} + \frac{1}{2}\int \sum_{\sigma} \frac{\partial \varphi^*}{\partial X_\sigma}\frac{\partial \chi}{\partial X_\sigma}\, d\boldsymbol{u}. \tag{A2.1}$$

The first term of (A2.1) becomes zero because of the boundary condition. Therefore, if we introduce the general coordinate, $\boldsymbol{q}$, the matrix element (I) can be written as

$$I = \frac{1}{2}\int \sum_{j,k,\sigma} \frac{\partial q_j}{\partial X_\sigma}\frac{\partial \varphi^*}{\partial q_j}\frac{\partial q_k}{\partial X_\sigma}\frac{\partial \chi}{\partial q_k}\, d\boldsymbol{u} = \frac{1}{2}\int \sum_{j,k} a_{jk}^{-1}\frac{\partial \varphi^*}{\partial q_j}\frac{\partial \chi}{\partial q_k}\, d\boldsymbol{u}, \tag{A2.2}$$

where $\boldsymbol{a}^{-1}$ is defined as follows:

$$a_{jk}^{-1} \equiv \sum_{\sigma} \frac{\partial q_j}{\partial X_\sigma}\frac{\partial q_k}{\partial X_\sigma}. \tag{A2.3}$$

It can be easily shown that $\boldsymbol{a}$ takes the form

$$a_{jk} = \sum_{\sigma} \frac{\partial X_\sigma}{\partial q_j}\frac{\partial X_\sigma}{\partial q_k}. \tag{A2.4}$$

If we change the variables of the volume element in (A2.2) to $\boldsymbol{q}$, the final expression is obtained as

$$I = \frac{1}{2}\int \sum_{j,k} a_{jk}^{-1}\frac{\partial \varphi^*}{\partial q_j}\frac{\partial \chi}{\partial q_k} J\left(\frac{\boldsymbol{X}}{\boldsymbol{q}}\right) d\boldsymbol{q}, \tag{A2.5}$$

where J is an Jacobian defined as

$$J\left(\frac{\boldsymbol{X}}{\boldsymbol{q}}\right)=\sqrt{|\boldsymbol{a}|}. \tag{A2.6}$$

Appendix 3

The relationship among mass-weighted Cartesian coordinates, reaction coordinate and normal coordinates is

$$\boldsymbol{X}_i=\boldsymbol{S}_i(r)+\sum_{k=1}^{3N-7}\boldsymbol{L}_{ik}(r)Q_k \qquad (i=1,N) \tag{A3.1}$$

where $\boldsymbol{X}_i$ is a three-dimensional vector representing the mass-weighted Cartesian coordinates of atom i. Therefore, the derivatives of $\boldsymbol{X}$ with respect to r and $\boldsymbol{Q}$ are

$$\frac{\partial \boldsymbol{X}_\alpha}{\partial r}=\frac{\partial \boldsymbol{S}_\alpha(r)}{\partial r}+\sum_{k=1}^{3N-7}\frac{\partial \boldsymbol{L}_{\alpha k}(r)}{\partial r}Q_k, \tag{A3.2a}$$

$$\frac{\partial \boldsymbol{X}_\alpha}{\partial Q_i}=\boldsymbol{L}_{\alpha i}(r). \tag{A3.2b}$$

$\boldsymbol{a}$ can be calculated from (3.12a) as

$$a_{mn}=\sum_\sigma \frac{\partial X_\sigma}{\partial q_m}\frac{\partial X_\sigma}{\partial q_n}. \tag{A3.3}$$

The explicit form of $\boldsymbol{a}$ is as follows:

$$a_{rr}=c(r)+2\sum_i u_i(r)Q_i+\sum_{ij} v_{i,j}(r)Q_iQ_i, \tag{A3.4a}$$

$$a_{mm}=\beta_m(r) \qquad (m\neq r), \tag{A3.4b}$$

$$a_{rm}=a_{mr}=T_m(r)+\sum_{k=1}^{3N-7} w_{mi}(r)Q_i \qquad (m\neq r), \tag{A3.4c}$$

$$a_{mn}=0 \qquad (m\neq r, n\neq r, m\neq n), \tag{A3.4d}$$

$$\begin{aligned}|\boldsymbol{a}|=&(c(r)-y(r))R(r)+2\sum_{i=1}^{3N-7}(u_i(r)-z_i(r))R(r)Q_i\\&+\sum_{ij}^{3N-7}(v_{ij}(r)-\alpha_{ij}(r))R(r)Q_iQ_j,\end{aligned} \tag{A3.5}$$

where c, u, v, β, T, w, y, z, R, and α are defined as

$$c(r)=\sum_\alpha\left(\frac{\partial \boldsymbol{S}_\alpha(r)}{\partial r}\right)^2, \tag{A3.6a}$$

$$u_m(r)=\sum_\alpha \frac{\partial \boldsymbol{S}_\alpha(r)}{\partial r}\frac{\partial \boldsymbol{L}_{\alpha_m}(r)}{\partial r}, \tag{A3.6b}$$

$$v_{mn}(r) = \sum_{\alpha} \frac{\partial \boldsymbol{L}_{\alpha_m}(r)}{\partial r} \frac{\partial \boldsymbol{L}_{\alpha_n}(r)}{\partial r}, \tag{A3.6c}$$

$$\beta_m(r) = \sum_{\alpha} \boldsymbol{L}^2_{\alpha_m}(r), \tag{A3.6d}$$

$$T_m(r) = \sum_{\alpha} \frac{\partial \boldsymbol{S}_{\alpha}(r)}{\partial r} \boldsymbol{L}_{\alpha_m}(r), \tag{A3.6e}$$

$$w_{mn}(r) = \sum_{\alpha} \boldsymbol{L}_{\alpha_m}(r) \frac{\partial \boldsymbol{L}_{\alpha_n}(r)}{\partial r}, \tag{A3.6f}$$

$$y(r) = \sum_{i} \frac{T_i^2(r)}{\beta_i(r)}, \tag{A3.6g}$$

$$z_m(r) = \sum_{i} \frac{T_i(r) w_{im}(r)}{\beta_i(r)}, \tag{A3.6h}$$

$$R(r) = \prod_{i} \beta_i(r), \tag{A3.6i}$$

$$\alpha_{mn}(r) = \sum_{i} \frac{w_{im}(r) w_{in}(r)}{\beta_i(r)}. \tag{A3.6j}$$

The inverse of $\boldsymbol{a}$ can be obtained analytically. It is

$$(a^{-1})_{rr} \cdot |\boldsymbol{a}| = R(r), \tag{A3.7a}$$

$$\begin{aligned}(a^{-1})_{mm} \cdot |\boldsymbol{a}| = {} & \frac{R(r)}{\beta_m(r)} \left(c(r) - y(r) + \frac{T_m^2(r)}{\beta_m(r)} \right) \\ & + 2 \frac{R(r)}{\beta_m(r)} \sum_{i} \left(u_i(r) - z_i(r) + \frac{T_m(r) w_{mi}(r)}{\beta_m(r)} \right) Q_i \\ & + \frac{R(r)}{\beta_m(r)} \sum_{ij} \left(v_{ij}(r) - \alpha_{ij}(r) + \frac{w_{mi}(r) w_{mj}(r)}{\beta_m(r)} \right) Q_i Q_j \quad (m \neq r),\end{aligned} \tag{A3.7b}$$

$$(a^{-1})_{rm} \cdot |\boldsymbol{a}| = (a^{-1})_{mr} \cdot |\boldsymbol{a}| = - \frac{R(r) T_m(r)}{\beta_m(r)} - \frac{R(r)}{\beta_m(r)} \sum_{i} w_{mi}(r) Q_i \quad (m \neq r), \tag{A3.7c}$$

$$\begin{aligned}(a^{-1})_{mn} \cdot |\boldsymbol{a}| = {} & - \frac{R(t) T_m(r) T_n(r)}{\beta_m(r) \beta_n(r)} + \frac{R(r)}{\beta_m(r) \beta_n(r)} \sum_{i} (T_m(r) w_{ni}(r) + T_n(r) w_{mi}(r)) Q_i \\ & + \frac{R(r)}{\beta_m(r) \beta_n(r)} \sum_{ij} w_{mi}(r) w_{nj}(r) Q_i Q_j \quad (m \neq r, n \neq r, m \neq n).\end{aligned} \tag{A3.7d}$$

Appendix 4

The second-order Taylor expansions of (A3.7) are

$$(a^{-1})_n J = (1-y(r))^{-1/2} - (1-y(r))^{-3/2} \sum_i (u_i(r) - z_i(r)) Q_i + \tfrac{1}{2}(1-y(r))^{-3/2} \sum_{i,j} \left[\alpha_{ij}(r) - v_{ij}(r) + \frac{3(u_i(r) - z_i(r))(u_j(r) - z_j(r))}{1-y(r)} \right] Q_i Q_j, \tag{A4.1a}$$

$$(a^{-1})_{mm} J (1-y(r))^{1/2} + (1-y(r))^{-1/2} T_m^2(r) \qquad (m \neq r), \tag{A4.1b}$$

$$(a^{-1})_{rm} J = (a^{-1})_{mr} J = -(1-y(r))^{-1/2} T_m(r) + (1-y(r))^{-1/2} \sum_i \left[\frac{T_m(r)(u_i(r) - z_i(r))}{(1-y(r))} - w_{mi}(r) \right] Q_i \qquad (m \neq r), \tag{A4.1c}$$

$$(a^{-1})_{mn} J = (1-y(r))^{-1/2} T_m(r) T_n(r) \qquad (m \neq r, n \neq r, m \neq n). \tag{A4.1d}$$

The Taylor expansion of the Jacobian, J is

$$J = (1-y(r))^{1/2} + (1-y(r))^{-1/2} \sum_i (u_i(r) - z_i(r)) Q_i + \tfrac{1}{2}(1-y(r))^{-1/2} \sum_{i,j} \left[v_{ij}(r) - \alpha_{ij}(r) - \frac{(u_i(r) - z_i(r))(u_j(r) - z_j(r))}{1-y(r)} \right] Q_i Q_j. \tag{A4.1e}$$

Appendix 5

The gradient, $\boldsymbol{g}$ is expressed as

$$\boldsymbol{g} = \frac{\partial V}{\partial \boldsymbol{x}} = \sum_i \frac{\partial q_i}{\partial \boldsymbol{x}} \frac{\partial V}{\partial q_i}, \tag{A5.1}$$

where $\boldsymbol{q}$ are general coordinates (in this case $\{r, \boldsymbol{Q}\}$). From (3.2), the potential energy for the steepest descent reaction path is written as

$$V(r, \boldsymbol{Q}) = V_0(r) + \sum_{k=1}^{3N-7} \tfrac{1}{2} \omega_k^2(r) Q_k^2. \tag{A5.2}$$

The derivatives of V with respect to r and Q are thus obtained as

$$g_r \equiv \frac{\partial V}{\partial r} = \frac{\partial V_0(r)}{\partial r} + \sum_{k=1}^{3N-7} \omega_k(r) \frac{\partial \omega_k(r)}{\partial r} Q_k^2, \tag{A5.3a}$$

$$g_Q \equiv \frac{\partial V}{\partial \boldsymbol{Q}} = \omega(r)^2 \boldsymbol{Q}. \tag{A5.3b}$$

The square norm of the gradient is expressed as

$$(\boldsymbol{g}^2) = \begin{pmatrix} g_r^T \\ \boldsymbol{g}_Q^T \end{pmatrix} \boldsymbol{a}^{-1} (g_r \boldsymbol{g}_Q), \tag{A5.4}$$

where $\boldsymbol{a}^{-1}$ is (A2.7a)–(A2.7d) with the constraints in (3.14a) and (3.14b). The (approximate) form of $\boldsymbol{a}^{-1}$ is

$$a_{rr}^{-1} = \frac{1}{\left(1 + \sum_i u_i(r) Q_i\right)^2}, \tag{A5.5a}$$

$$a_{r\boldsymbol{Q}}^{-1} = a_{\boldsymbol{Q}r}^{-1} \approx 0, \tag{A5.5b}$$

$$a_{\boldsymbol{Q}\boldsymbol{Q}'}^{-1} \approx \delta_{\boldsymbol{Q}\boldsymbol{Q}'}, \tag{A5.5c}$$

where non-adiabatic and higher order terms are neglected. The square norm of $\boldsymbol{g}$ is now calculated from (A5.3a)–(A5.5c). It is

$$(\boldsymbol{g}^2) = \left(\frac{\partial V_0(r)}{\partial r}\right)^2 - 2\left(\frac{\partial V_0(r)}{\partial r}\right)^2 \sum_i u_i Q_i + 2 \frac{\partial V_0(r)}{\partial r} \sum_i \omega_i(r) \frac{\partial \omega_i(r)}{\partial r} Q_i^2 + \sum_i \omega_i^4(r) Q_i^2. \tag{A5.6}$$

Therefore, the derivative of $\boldsymbol{g}^2$ with respect to $\boldsymbol{Q}$ can be evaluated as

$$\frac{\partial(\boldsymbol{g}^2)}{\partial Q_i} = -2\left(\frac{\partial V_0(r)}{\partial r}\right)^2 u_i(r) + 2 \frac{\partial V_0(r)}{\partial r} \omega_i(r) \frac{\partial \omega_i}{\partial r} Q_i + 2\omega_i^4(r) Q_i. \tag{A5.7}$$

References

1. Hofacker GL, Seiler R (1969) J Chem Phys 51:3951
2. Marcus RA (1966) J Chem Phys 45:4493:4500
3. Fukui K (1970) J Phys Chem 74:4161; see also Fukui K (1971) Acc Chem Res 14:368
4. a. Tachibana A, Fukui K (1978) Theor Chim Acta 49:321
   b. Tachibana A, Fukui K (1980) Theor Chim Acta 57:81
5. a. Yamashita K, Yamabe T, Fukui K (1981) Chem Phys Lett 84:123
   b. Yamashita K, Yamabe T, Fukui K (1982) Theor Chim Acta 60:523
   c. Yamabe K, Koizumi M, Yamashita K, Tachibana T (1984) J Am Chem Soc 106:2255
6. a. Truhlar DG, Garrett BC (1980) Acc Chem Res 13:440
   b. Truhlar DG, Garrett BC (1984) Ann Rev Chem 35:159
   c. Truhlar DG, Garrett BC (1984) J Chim Phys 84:1

7. a. Miller WH, Handy NC, Adams JE (1980) J Chem Phys 72:99
   b. Carrington Jr. T, Miller WH (1986) J Chem Phys 84:15
   c. Makki N, Miller WH (1987) J Chem Phys 86:1451
8. Hougen JH, Bunker PR, Johns WC (1970) J Mol Spectrosc 34:136
9. Panicir J (1975) Collect Czech Chem Commun 40:1112
10. Müller K (1980) Angew Chem Int Ed Engl 19:1
11. Basilevsky MV, Shamov AG (1981) Chem Phys 60:347
12. Hoffman DK, Nord RS, Ruedenberg K (1986) Theor Chim Acta 69:265
13. Jørgensen P, Aa. Jensen HJ, Helgaker T (1988) Theor Chim Acta 73:55
14. Simons J, Jørgensen P, Taylor H, Ozment J (1985) J Phys Chem 89:4020
15. a. Gray SK, Miller WH, Yamaguchi Y, Schaefer III HF (1980) J Chem Phys 73:2733
   b. Osamura Y, Schaefer III HF, Gray SK, Miller WH (1981) J Am Chem Soc 103:1904
   c. Waite BA, Gray SK, Miller WH (1983) J Chem Phys 78:259; see also [7]
16. a. Truhlar DG, Isaacson, AD, Skodje RT, Garrett, BC (1982) J Chem Phys 86:2252
   b. Garrett BC, Truhlar DG, Wagner AF, Dunning Jr. TH (1983) J Chem Phys 78:4400
   c. Skodje RT, Schwenke DW, Truhlar DG, Garrett BC (1984) J Am Chem Soc 88:628
   d. Brown FB, Tucker SC, Truhlar DG (1985) J Chem Phys 83:4451
   e. Garrett BC, Abusalbi N, Kouri DJ, Truhlar DG (1985) J Chem Phys 83:2242
   f. Garrett BC, Truhlar DG, Bowman JM, Wagner AF (1986) J Phys Chem 90:4305
   g. Hancock GC, Rejto PR, Steckler R, Brown FB, Schwenke DW, Truhlar DG (1986) J Chem Phys 85:4997
   h. Joseph T, Steckler R, Truhlar DG (1987) J Chem Phys 87:7036
17. Eckart C (1935) Phys Rev 47:552
18. Goldstein H (1950) Classical mechanics. Addison-Wesley, Reading
19. Wilson Jr. EB, Decius JC, Cross PC (1955) Molecular vibrations. McGraw-Hill, New York, p 283
20. Löwdin PO (1950) J Chem Phys 18:365
21. Stevens RM (1971) J Chem Phys 55:1725
22. Tatewaki H (1985) J Comput Chem 6:237
23. Benedict WS, Plyler EK (1957) Can J Phys 35:1235
24. Tatewaki H, Huzinaga S (1980) J Comput Chem 3:205
25. Botschwina P, Rosmus P, Reinsch EA (1983) Chem Phys Lett 104:299;
   Shida N, Tanaka K, Ohno K (1986) In: Smith VH (ed) Applied quantum chemistry. Reidel, Dordrecht
26. The program code was written by Aa. Jensen HJ, Ågren H, Jørgensen P (private communication)
27. The program code was written by Halgaker T, Jørgensen P, Aa. Jensen HJ (private communication)